

Statistically robust linear and nonlinear wavelet analysis applied to plasma edge turbulence

B. Ph. van Milligen, C. Hidalgo, E. Sánchez, M. A. Pedrosa, R. Balbín,
and I. García-Cortés

Asociacion Euratom-CIEMAT, Madrid, Spain

G. R. Tynan

Institute for Plasma and Fusion Research, University of California, Los Angeles, California 90024

(Presented on 15 May 1996)

The analysis of turbulence requires adequate analysis tools. In particular, two general properties of turbulence make the application of standard analysis tools (spectral analysis) difficult: (1) intermittency, which causes the characteristics of turbulence to change on a relatively short time scale, implies that analysis tools must not integrate over time scales longer than the intermittent time scale; (2) nonlinearity, a basic property of all numerical models of chaos and turbulence, requires specially adapted tools for its proper detection. In the present work, we develop a statistically stable formalism for the application of wavelet analysis techniques to the analysis of turbulence. We apply these techniques to the analysis of Langmuir probe data in the plasma edge region of the TJ-IU Torsatron. We draw some tentative conclusions about radial correlation lengths. Further, we analyze the L/H transition at the Continuous Current Tokamak and reconstruct a radial profile of bicoherence in the plasma edge in the H-mode. © 1997 American Institute of Physics.

[S0034-6748(97)65601-4]

I. INTRODUCTION

Although the phenomenon of turbulence is only partially understood, there seems to be consensus on several aspects. First, that *intermittency* is a basic property of turbulence. This means that the characteristics of the turbulence (spectral distribution, amplitude, etc.) vary on a short time scale. Analysis techniques that rely on the accumulation of data over time scales larger than this characteristic time scale will then average out much of the dynamics and obliterate relevant information (as may occur with Fourier analyses).

Wavelet analysis is ideally suited to tackle this problem. Standard wavelet analysis is, however, not fully adequate since it is not statistically robust. In this article, we shall develop statistically stable wavelet techniques.

Second, it is generally accepted that turbulence only arises in nonlinear systems. Therefore, to understand the nature of turbulence, it is essential to employ analysis tools that are capable of handling this nonlinearity. The usual analyses based on (cross-) spectra and (cross-) correlations, essentially linear analysis techniques, are not adequate.

Nonlinear analysis tools can be obtained by generalizing the common spectral analysis methods to higher order, which then are sensitive to nonlinear interactions. We focus on the so-called bispectral analysis, a method for the detection of quadratic interactions. Statistical stability of the bispectrum—a third-order spectrum—is again an important point, and noise level estimates can be provided. The main application of the bispectrum is the detection of phase coupling. It has been shown in earlier publications^{1,2} how reasonable time resolution, relevant to intermittency in some turbulent phenomena, can be achieved. Also it has been discussed how the bicoherence is related to nonlinearity and the presence of structure in turbulence.

II. SPECTRAL ANALYSIS TOOLS

In this section, we give a statistically robust definition of the wavelet cross spectrum and cross coherence.

A. Wavelet analysis

In the present work, we use the continuous wavelet transform based on the Morlet wavelet which has the benefit of conceptual closeness to the Fourier analysis base functions $e^{-i\omega t}$:

$$\Psi(t) = \pi^{-1/4} \exp[-i2\pi t - \frac{1}{2}t^2]; \quad \Psi_a(t) = a^{-1/2}\Psi(t/a). \quad (1)$$

We assign a frequency $\omega=2\pi/a$ to each scale a . The frequency resolution of the wavelet $\Psi_a(t)$ is $\sim\Delta\omega=\omega/4$, and the time resolution is $\Delta t=2a$. Note that $\Delta\omega\times\Delta t=\pi$, independent of a .

The wavelet transform of a function $f(t)$ is defined by^{3,4}

$$W_f(a, \tau) = \int f(t)\Psi_a(t-\tau)dt. \quad (2)$$

The advantage of the wavelet analysis lies in the fact that the time resolution is variable with frequency, so that high frequencies have a sharper time resolution. Thus, turbulent signals are decomposed into oscillations that die out in time, and more rapidly so the higher their frequency, which seems more natural for turbulence than the Fourier picture of stationary oscillations.

B. Statistically robust wavelet spectral analysis

In order to obtain statistical stability for our spectral analysis tools while maintaining time resolution, we average appropriate combinations of wavelet coefficients over a (small) finite time interval $T:\{T_0-T/2\leq\tau\leq T_0+T/2\}$. This procedure allows the estimation of a noise level which will tell us the statistical significance of the obtained results.

Thus, e.g., the wavelet cross spectrum is given by

$$C_{fg}^w(a, T_0) = \int_T W_f^*(a, \tau) W_g(a, \tau) d\tau, \quad (3)$$

where $f(t)$ and $g(t)$ are two time series and C_{fg}^w is complex. The normalized wavelet cross coherence is

$$\gamma_{fg}^w(a, T_0) = \frac{|\int_T W_f^*(a, \tau) W_g(a, \tau) d\tau|}{(P_f^w(a, T_0) P_g^w(a, T_0))^{1/2}} \quad (4)$$

which can take on values between 0 and 1. Here the wavelet auto-power spectrum is $P_f^w(a, T_0) = C_{ff}^w(a, T_0)$.

To calculate γ_{fg}^w [Eq. (4)], the wavelet coefficients are determined for each of $N = T \times f_{\text{samp}}$ samples in the interval T and averaged [Eq. (2)], where $\omega_{\text{samp}} = 2\pi f_{\text{samp}}$ is the sampling frequency. However, these wavelet coefficients are not all statistically independent, since the chosen wavelet family is not orthogonal. Due to the periodicity a of the wavelets, two statistically independent estimates of the wavelet coefficients are separated by a time $a/2$, or by a number of points $M(a) = a \times \omega_{\text{samp}} / 4\pi$. Thus, the integral appearing in Eq. (2) is carried out over $N/M(a)$ independent estimates of wavelet coefficients. Using this, we may estimate the statistical noise level as

$$\epsilon[\gamma_{fg}^w(a, T_0)] \approx 2 \left[\frac{\omega_{\text{samp}}}{\omega} \frac{1}{N} \right]^{1/2}. \quad (5)$$

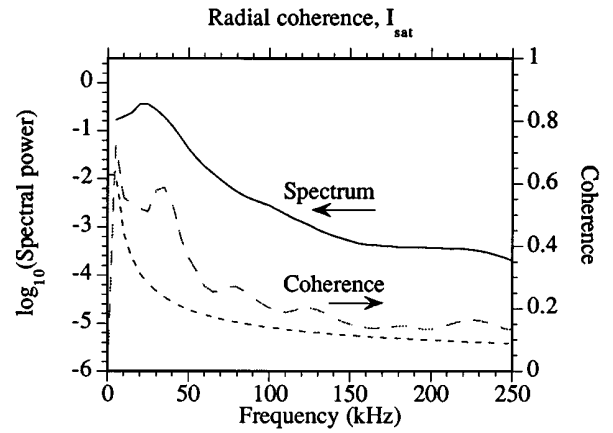
The value of γ_{fg}^w as obtained for Gaussian noise conforms quite well to this prediction.

Similar definitions can be given for higher-order spectra that measure the presence of nonlinear interactions. Refer to Refs. 1 and 2 for the corresponding definitions.

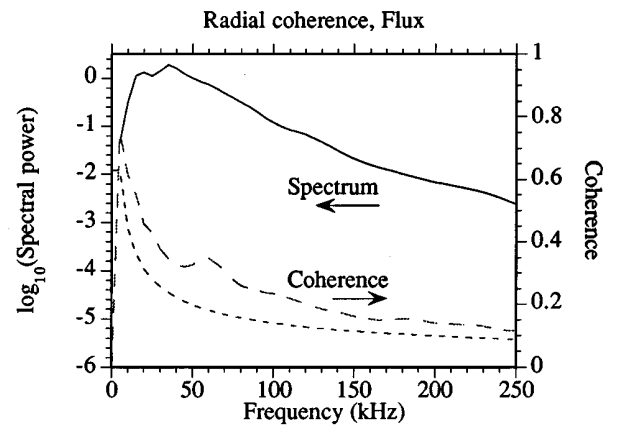
III. RADIAL COHERENCE OBSERVED ON THE TJ-IU TORSATRON

The time-resolved radial turbulent flux, $\Gamma_T = \tilde{n} \tilde{E}_\theta / B_T$, was measured at two radially separated positions (separation 1 cm) in the plasma edge region of the TJ-IU Torsatron.⁵ The plasmas were heated by electron cyclotron resonance heating (ECRH), and have $R=0.6$ m, central rotational transform $\iota(0)=0.21$, $\langle a \rangle = 0.1$ m, $B_i = 0.6$ T, and $n_e = 5 \times 10^{18} \text{ m}^{-3}$. Each of the two probes has three tips, aligned perpendicular to the magnetic field and separated poloidally by $\Delta = 0.2$ cm. The probes were designed and positioned to avoid shadowing effects.⁶ The fluctuating poloidal electric field is then derived from the measured fluctuating floating potential in the two most extreme probe tips: $\tilde{E}_\theta = [\tilde{\Phi}_f(1) - \tilde{\Phi}_f(2)] / \Delta$. The third probe tip is located between the other two, but slightly displaced toroidally. It is set up to measure the ion saturation current I_{sat} . The turbulent flux Γ_T has been calculated neglecting the influence of temperature fluctuations ($\tilde{n} \propto \tilde{I}_{\text{sat}}$). The signals are sampled at 1 MHz.

Figure 1(a) shows the cross spectrum and radial cross correlation between the \tilde{I}_{sat} signals of the two radially separated probes. The influence of a magnetohydrodynamics (MHD) mode is recognized in the peak of the spectrum at about 20 kHz. The cross correlation peaks at slightly higher frequency (35 kHz).



(a)



(b)

FIG. 1. (a) Cross spectrum and cross coherence of I_{sat} from two radially separated probes in the edge zone of a TJ-IU discharge. Continuous line: average wavelet spectrum; long dashes: wavelet coherence; short dashes: the noise level of the coherence. (b) Same for the instantaneous particle flux derived from the probe data (see the text). The value of the coherence is smaller than for I_{sat} .

Figure 1(b) shows the same graph, now calculated for Γ_T . Features similar to the ones observed in Fig. 1(a) can be seen, although at higher frequencies. This frequency shift is easily explained by the fact that Γ_T is a quadratic signal. What is most interesting is that the flux does not show a larger radial correlation than \tilde{I}_{sat} (or $\tilde{\Phi}_f$ either, not shown).

Figure 2 shows the temporally resolved coherence of \tilde{I}_{sat} . The time resolution is 0.5 ms. The noise level is the same as in Fig. 1. The coherence is highly intermittent and occasionally very high values are achieved (much higher than the time-average value).

IV. BICOHERENCE PROFILE AT THE L/H TRANSITION ON CCT

The data analyzed in this section are from the continuous current tokamak (CCT). It was operated with $R=1.5$ m, $a=0.35$ m, $B_i=0.25$ T, $I_p \approx 40$ kA, $n_e = 2 \times 10^{18} \text{ m}^{-3}$, $V_{\text{loop}} = 1.2-1.4$ V, $T_e(0) > 150$ eV, and $T_i(0) > 100$ eV. H modes were induced by biasing a small electrode located about 0.1 m inside the limiter radius with respect to the vessel wall.⁷

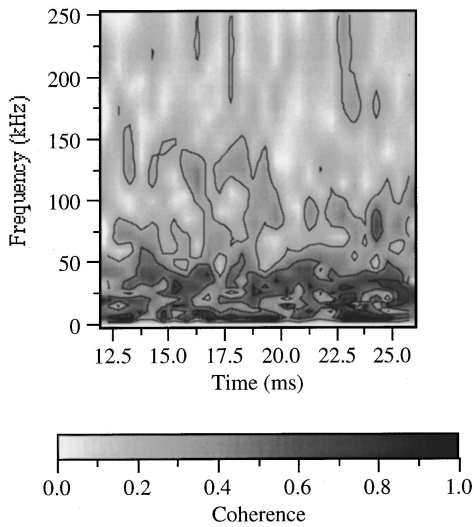


FIG. 2. Time-resolved wavelet coherence-versus-time graph of I_{sat} . The coherence is between two radially separated probes (see the text). The noise level is the same as in Fig. 1. In several time intervals and at various frequencies the coherence obtains values far above the time-average value.

For studies of edge turbulence and transport, a poloidal Langmuir probe array was used.^{8,9} It was configured such that one of the probe tips was recording the floating potential locally. The sampling rate was 2.5 MHz. Here we focus on data from a Langmuir probe located at the outside midplane. Prior to the initiation of H mode, the probe was located just outside the last-closed-flux-surface (LCFS). During H modes, the increasing plasma pressure causes a slow movement of the plasma column out towards the low-field side. Thus, when the H mode electrode bias is suddenly turned on, the outside midplane probe records a slow increase in the negative dc floating potential. This enabled us to reconstruct the radial profile in the H mode of the quantities measured by the probe using an estimate of the instantaneous probe position relative to the LCFS. Knowing the value of the radial electric field E_r , the radial position r of the probe can be estimated as $r = \Phi_f / E_r$, where Φ_f is the floating potential measured by the probe. From Doppler shift measurements, we estimated the electric field to be $E_r \sim -100$ V/cm. Uncertainties in this estimate translate into an uncertainty of 30%–50% in the absolute reconstructed position, although the relative position is much more accurate since E_r does not vary significantly during the measurements.

Figure 3 shows the rms values and the bicoherence of the measured ion saturation current (I_{sat}) for the outside midplane probe. The H -mode period (gray area) shows a slight reduction of the rms and a gradual increase of the bicoherence as the plasma moves outward. A broad range of frequencies is involved in the production of the high bicoherence around $t=80$ ms, with predominance of frequencies around 250 and 500 kHz.

Observations reported earlier for L/H transitions (using reflectometry)² showed an abrupt increase of the bicoherence and decrease of the rms at the transition. The difference with the present apparently smooth transition may be explained by the fact that here the probe location is initially at the LCFS and moves gradually inward, whereas in the measure-

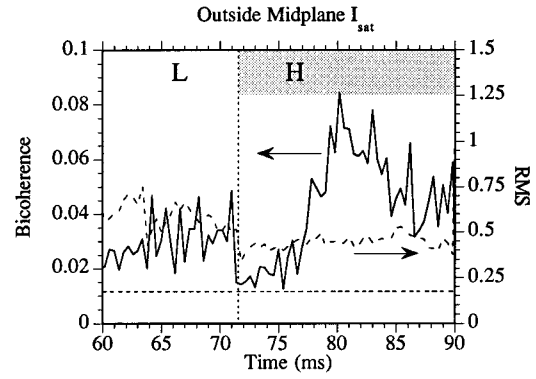


FIG. 3. Analysis of the saturation current I_{sat} measured by a Langmuir probe positioned on the outside midplane at CCT. Long dashes: rms of I_{sat} . Drawn line: bicoherence of I_{sat} . Short dashes: Noise level of the bicoherence. The gray area indicates the H -mode period, induced by probe biasing.

ments reported earlier the measurements were taken well inside the LCFS. This would imply that the gradual change observed is due rather to the existence of a bicoherence profile than to a slow temporal change.

Performing standard statistical analysis on the outside midplane \tilde{I}_{sat} signal, we calculate the probability distribution function (PDF) before and after the transition. Calculations are performed on records of 12 500 samples after high-pass digital filtering with a cutoff frequency 1 kHz to remove drifts. We find that the L -mode PDF is Poisson-like (with skewness $S > 1$, and kurtosis $K > 5$), whereas in the H mode it is more like a Gaussian ($0 < S < 1$, $3 < K < 4$) (Fig. 4). The deviation from gaussianity in the L mode as contrasted with the near gaussianity in the H mode is consistent with earlier studies of the relation between the PDF shape of turbulent signals and plasma conditions.¹⁰

Using the above-mentioned estimate of the probe position, the profile of bicoherence was reconstructed during the H -mode phase from the signal of the outside midplane probe. The result is shown in Fig. 5, along with a similar profile obtained from a different but similar discharge. We recall that a high value of the bicoherence may either indicate the presence of nonlinear interactions or of (quasistatic) structure.¹¹ It is interesting that these features should occur a

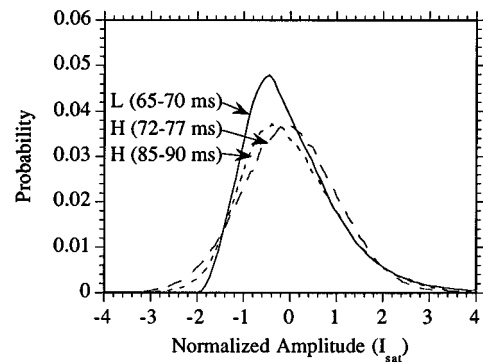


FIG. 4. PDF of the outside midplane \tilde{I}_{sat} signal in the L mode and the H mode. L mode (65–70 ms): Skewness $S=1.32 \pm 0.07$, Kurtosis $K=5.94 \pm 0.22$; H mode (72–77 ms): $S=0.15 \pm 0.06$, $K=3.27 \pm 0.11$; H mode (85–90 ms): $S=0.67 \pm 0.06$, $K=3.83 \pm 0.13$.

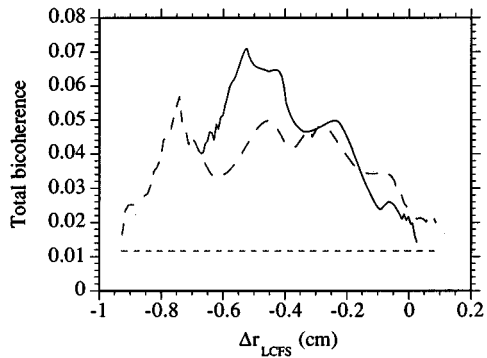


FIG. 5. Bicoherence profile in the H mode deduced from the outside mid-plane probe signal shown in Fig. 3 and an estimate of the probe position relative to the LCFS (continuous line). Also included is a similar profile for another, similar discharge (long dashes). The noise level of the bicoherence is indicated by the short-dashed line.

small distance inside and not at the LCFS, which is possibly related to a (decorrelating) velocity shear layer at the LCFS. The results also seem to indicate a *maximum* of bicoherence about half a cm inside the LCFS. The meaning of this fea-

ture, reported for the first time here, is as yet unclear but may have bearing on H -mode physics.

- ¹B. Ph. van Milligen, C. Hidalgo, and E. Sánchez, Phys. Rev. Lett. **74**, 395 (1995).
- ²B. Ph. van Milligen, E. Sánchez, T. Estrada, C. Hidalgo, B. Brañas, B. Carreras, and L. García, Phys. Plasmas **2**, 3017 (1995).
- ³C. Chui, *An Introduction to Wavelets* (Academic, New York, 1992).
- ⁴I. Daubechies, Ten Lectures on Wavelets, National Science Foundation Series In Applied Mathematics, S.I.A.M. 1992 (unpublished).
- ⁵E. Ascasíbar *et al.* Plasma Phys. Control. Nucl. Fusion Research, IAEA-CN-60/A6-1, **1**, 749 (1994).
- ⁶M. A. Pedrosa, C. Hidalgo, B. van Milligen, E. Sánchez, R. Balbín, I. García-Cortés, H. Niedermeyer, and L. Giannone, Proceedings of the 23rd European Conference Kiev, 1996 (unpublished).
- ⁷R. J. Taylor, M. L. Brown, B. D. Fried, H. Grote, J. R. Liberati, G. J. Morales, P. Pribyl, D. Darrow, and M. Ono, Phys. Rev. Lett. **63**, 2365 (1989).
- ⁸G. R. Tynan, Ph.D. thesis, School of Engineering, University of California, Los Angeles, 1991.
- ⁹G. R. Tynan, L. Schmitz, R. W. Conn, R. Doerner, and R. Lehmer, Phys. Rev. Lett. **68**, 3032 (1992).
- ¹⁰B. A. Carreras, C. Hidalgo, E. Sánchez, M. A. Pedrosa, R. Balbín, I. García-Cortés, B. Ph. van Milligen, D. E. Newman, and V. E. Lynch, Phys. Plasmas **3**, 2664 (1996).
- ¹¹H. L. Pécseli and J. Trulsen, Plasma Phys. Control. Fusion **35**, 1701 (1993).